

## Role of temperature and Coulomb correlation in the stabilization of the CsCl-type phase in FeS under pressure

Alexey O. Shorikov,<sup>1,2,\*</sup> Valery V. Roizen,<sup>3</sup> Artem R. Oganov,<sup>3,4</sup> and Vladimir I. Anisimov<sup>1,2</sup>

<sup>1</sup>*M.N. Miheev Institute of Metal Physics of Ural Branch of Russian Academy of Sciences - 620990 Yekaterinburg, Russia*

<sup>2</sup>*Ural Federal University - 620002 Yekaterinburg, Russia*

<sup>3</sup>*Moscow Institute of Physics and Technology, 9 Institutskiy per., Dolgoprudny, Moscow Region, 141701, Russia*

<sup>4</sup>*Skolkovo Institute of Science and Technology, 3 Nobel Street, Moscow, 143026, Russia*



(Received 2 November 2017; revised manuscript received 17 August 2018; published 25 September 2018)

The iron-sulfur system is important for planetary interiors and is intensely studied, particularly for better understanding of the cores of the Earth and of terrestrial planets. Yet, there is a paradox about high-pressure stability of FeS: *ab initio* global optimization (at DFT level) predicts a  $Pm\bar{m}n$  phase (with a distorted rocksalt structure) to be stable at pressures above  $\sim 120$  GPa, which has not yet been observed in the experiments, which instead revealed a CsCl-type phase which, according to density functional calculations, should not be stable. Using quasiharmonic free energy calculations and dynamical mean-field theory, we show that this apparent discrepancy is removed by proper account of electron correlations and entropic effects.

DOI: [10.1103/PhysRevB.98.094112](https://doi.org/10.1103/PhysRevB.98.094112)

### I. INTRODUCTION

The composition of the Earth's core is a topic of intense research. The main components of the Earth's core, iron and nickel, are mixed with a small amount of lighter elements [1]. However, the chemical composition and crystal structure of the core compounds are still a subject of discussion. Sulfur is seen as one of the preferred candidates to be present in the core [2] and  $\text{Fe}_{1-x}\text{S}$  is one of the most common sulfides on Earth (encountered also in lunar and meteoric samples [3–7]). FeS exhibits rich polymorphism and its magnetic properties and phase diagram under high pressure have been investigated through both high-pressure experiments and *ab initio* simulations in numerous previous studies [3,5,8–23].

Stoichiometric FeS has a NiAs-type (B8) hexagonal structure (troilite, FeS I) at ambient conditions with  $P\bar{6}2c$  space group [17]. The onset of long-range magnetic order is observed at  $T_N \sim 600$  K. Previous experimental studies demonstrate a series of phase transitions with increasing pressure at room temperature; troilite transforms to a MnP-type structure (FeS II) with the orthorhombic space group  $Pnma$  above 3.4 GPa [8,24] and further to a monoclinic structure (FeS III) above 6.7 GPa. This transition is accompanied by a lattice volume collapse [4] and a change in the crystal symmetry (FeS III has space group  $P2_1/a$ ). The structural change from FeS II to III involves abrupt breaking of the long-range magnetic order [10,17,25], spin transition of iron, and metal-semiconductor transition. FeS IV (hexagonal superstructure of the NiAs-type) and FeS V (NiAs-type structure) are also known to exist at high pressures and temperatures. A phase transition to FeS VI with  $Pnma$  space group (MnP type) was found to occur above 30 GPa and 1300 K [26]. *Ab initio* calculations at higher pressures predicted transformation from the monoclinic phase of FeS to CsCl-type (B2) phase (FeS

VII) with  $Pm\bar{3}m$  space group [19]. This result has been confirmed by experiment: the CsCl-type phase was synthesized at 1300 K and 186 GPa [27].

However, there is a contradiction with more recent band-structure calculations [28] which predicted another phase with  $Pm\bar{m}n$  symmetry to be stable, while the CsCl-type structure was predicted to be metastable at 0 K (by 0.1–0.15 eV/atom) (Fig. 1). It should be noted that the CsCl-type phase is stable at high pressures in other iron alloys, such as FeSi [29].

Such discrepancy between theoretical and experimental results is quite intriguing. One can assume that the CsCl-type phase is stabilized by thermal effects. The results of Gibbs free energy calculations within the quasiharmonic approximation confirmed this hypothesis to a certain degree, while placing the CsCl-type phase stability field much higher in terms of pressure and temperature in comparison with the experimental data [30]. Such a difference cannot be put down to numerical errors, and that is why we hypothesized that Coulomb correlations too may be crucial in the stabilization of the CsCl-type phase. To confirm this, we conducted calculations by combining the generalized gradient approximation and dynamical mean-field theory (DFT+DMFT). Phonon calculations were run using the finite displacements method and allowed us to take thermal effects into account. Combining the results of our computational modeling, we calculated Gibbs free energy and constructed the ( $P$ ,  $T$ )-phase diagram.

### II. METHOD

In present work we have applied a combination of the state-of-the-art DMFT method with accounting for vibrational entropy to describe structural transitions. First, we relaxed the three crystal structures under investigations (namely  $Pnma$ ,  $Pm\bar{m}n$ , and CsCl type) at a number of pressures in a wide pressure range ( $-10 : 400$  GPa) using the VASP code [32]

\*Corresponding author: shorikov@imp.uran.ru

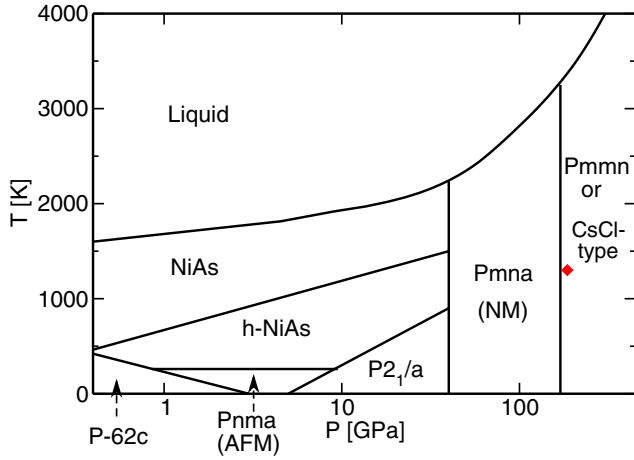


FIG. 1. Schematic phase diagram reproduced from Ref. [28]. Experimental point of CsCl-type phase [27] is shown with a red diamond.

(Fig. 2). We used the exchange-correlation potential in the form proposed by Perdew, Burke, and Ernzerhof [33]. PAW potentials with an [Ar] core (radius 2.3 a.u.) and [Ne] core (radius 1.9 a.u.) for Fe and S atoms, respectively, and a plane wave kinetic energy cutoff of 600 eV were used. Structure relaxations employed homogeneous-centered meshes with reciprocal space resolution of  $2\pi \times 0.02 \text{ \AA}^{-1}$  and Methfessel-Paxton electronic smearing with  $\sigma = 0.16 \text{ eV}$ . In order to take into account the correlation effects in the  $d$  shell of iron we applied the DFT+DMFT approach which exploits the advantages of two methods widely used nowadays: the noninteracting band structure  $\varepsilon(\vec{k})$  obtained within density functional theory (DFT) takes into account all the peculiarities of  $\varepsilon(\vec{k})$  for a given material, while dynamical mean-field theory (DMFT) takes care of many-body effects such as Coulomb correlations [34,35]. This method was successfully used in investigating different magnetic phenomena, including spin state transitions [36–39]. In contrast to LDA+ $U$  or GGA+ $U$  approaches, it allows both considering frequency dependence of the self-energy and simulating a paramagnetic state. The noninteracting GGA calculations were performed using the pseudopotential method as implemented in Quantum ESPRESSO [40]. We used the Wannier function projection procedure [41] to extract the noninteracting GGA Hamiltonian  $H_{\text{GGA}}$  which included both Fe 3d and S 2p states. The full many-body Hamiltonian to be solved by the

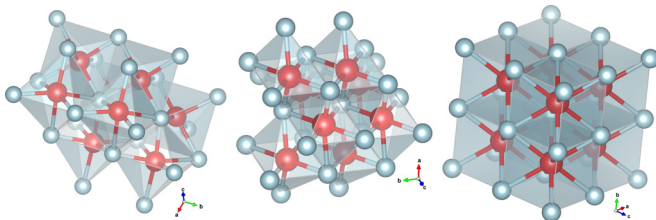


FIG. 2. Crystal structures of *Pnma* (left) *Pmmn* (middle), and CsCl-type (right) phases of FeS. Iron is shown with red and sulfur with blue balls. The crystal structures were drawn using VESTA [31].

DFT+DMFT is written in the form

$$\hat{H} = \hat{H}_{\text{GGA}} - \hat{H}_{\text{dc}} + \frac{1}{2} \sum_{i,m,m',\sigma,\sigma'} U_{m,m'}^{\sigma,\sigma'} \hat{n}_{i,m,\sigma} \hat{n}_{i,m',\sigma'}. \quad (1)$$

Here  $U_{m,m'}^{\sigma,\sigma'}$  is the Coulomb interaction matrix and  $\hat{n}_{i,m,\sigma}$  is the occupation number operator for the  $d$  electrons with orbitals  $m$  or  $m'$  and spin indexes  $\sigma$  or  $\sigma'$  on the  $i$ th site. The term  $\hat{H}_{\text{dc}}$  stands for the  $d$ - $d$  interaction already accounted for in DFT, the so-called double-counting correction which was chosen to be  $\hat{H}_{\text{dc}} = \bar{U}(n_{\text{dmft}} - \frac{1}{2})\hat{I}$  [34]. Here  $n_{\text{dmft}}$  is the self-consistent total number of  $d$  electrons obtained within DFT+DMFT and  $\bar{U}$  is the average Coulomb parameter for the  $d$  shell. The elements of  $U_{m,m'}^{\sigma,\sigma'}$  matrix are parametrized by  $U$  and  $J_H$  according to the procedure described in Ref. [42].

The effective impurity problem for the DMFT was solved by the hybridization expansion continuous-time quantum Monte Carlo method (CT-QMC) [43]. Calculations were performed for all the structures in the paramagnetic state at temperatures of 1160, 2000, 3000, 4000, and 5000 K, using the AMULET code [44]. For the sake of simplicity we used the same set of Coulomb parameters for all the structures and pressures (unit cells) under investigation. The on-site Hubbard  $U = 6 \text{ eV}$  and Hund's intra-atomic exchange  $J_H = 0.95 \text{ eV}$  were estimated in QE using constrained GGA calculations [45]. Note that these values agree well with the results of previous calculations of  $U$  for other Fe sulfides and oxides at high pressure [23,46] on the same Wannier functions which were applied to construct a small noninteracting Hamiltonian used in the subsequent DFT+DMFT calculations. Total energy was calculated within the DFT+DMFT as described in Ref. [47]:

$$E = E_{\text{GGA}} + \langle \hat{H}_{\text{GGA}} \rangle - \sum_{m,k} \epsilon_{m,k}^{\text{GGA}} + \frac{1}{2} \sum_{i,m,m',\sigma,\sigma'} U_{m,m'}^{\sigma,\sigma'} \langle \hat{n}_{i,m,\sigma} \hat{n}_{i,m',\sigma'} \rangle - E_{\text{dc}}. \quad (2)$$

Here  $E_{\text{GGA}}$  stands for the total energy obtained within GGA. The third term on the right-hand side of Eq. (2) is the sum of the Fe- $d$ , S- $p$  valence state eigenvalues calculated as the thermal average of the GGA Wannier Hamiltonian with GGA Green function  $\sum_{m,k} \epsilon_{m,k}^{\text{GGA}} = \frac{1}{\beta} \sum_{n,\mathbf{k}} \text{Tr}[H_{\text{GGA}}(\mathbf{k})G_{\mathbf{k}}^{\text{GGA}}(i\omega_n)]e^{i\omega_n 0^+}$ .  $\langle \hat{H}_{\text{GGA}} \rangle$  is evaluated in the same way but with the Green function which includes self-energy. The fourth term represents the interaction energy, here  $\langle \hat{n}_{i,m,\sigma} \hat{n}_{i,m',\sigma'} \rangle$  is the double occupancy matrix calculated in the DMFT. The double-counting correction  $E_{\text{dc}} = \frac{1}{2} \sum_{i,m,m',\sigma,\sigma'} U_{m,m'}^{\sigma,\sigma'} \langle \hat{n}_{i,m,\sigma} \rangle \langle \hat{n}_{i,m',\sigma'} \rangle$  corresponds to the average Coulomb repulsion between electrons in the Fe 3d Wannier orbitals calculated from the self-consistently determined local occupancies.

Vibrational entropy was calculated using the finite-displacement approach as implemented in the PHONOPY code [48,49]. First, supercells (typically  $2 \times 2 \times 2$ ) were constructed, and symmetrically inequivalent displacements of the atoms by  $0.01 \text{ \AA}$  performed. From the computed forces on atoms we constructed the dynamical matrix. Next, phonon frequencies and eigenvectors were obtained by solving the

dynamical matrix. A more detailed description of this technique is available elsewhere [48,49].

Combining results of DFMT and phonon calculations we were able to construct the phase diagram in  $(P, T)$  coordinates. For this purpose, we computed Gibbs free energies of the studied FeS phases. We addressed the task based on the following reasoning:

$$F(V, T) = E_{\text{elect}}(V, T) + F_{\text{vib}}(V, T), \quad (3)$$

$$E_{\text{elect}}(V, T) = E_{\text{DFT}}(V) + E_{\text{DMFT}}(V, T). \quad (4)$$

The first term in Helmholtz free energy [Eq. (3)] comes from an electron subsystem and can be calculated as the sum of total energy calculated within DFT and correction energy calculated within DMFT which takes into account electron-electron correlation effects [Eq. (4)]. The second term in Eq. (3) corresponds to vibration energy and can be calculated as

$$F_{\text{vib}}(V, T) = E_{z_p}(V) + \int_0^T C_V dT + S_{\text{vib}}(V, T)T. \quad (5)$$

The pressure can be determined as

$$P = -\frac{\partial F(V, T)}{\partial V} = P_{\text{elect}}(V, T) + P_{\text{vib}}(V, T). \quad (6)$$

The equations of state for electron energy were fitted using the Vinet equation of state [50], while phonon (Helmholtz) free energy was fitted by a third-order polynomial function. Next we calculate Gibbs free energy to construct the whole phase diagram:

$$G(P, T) = F(V, T) + P(V, T)V. \quad (7)$$

A similar approach for construction of the phase diagram was used by us earlier [30].

### III. RESULTS AND DISCUSSION

As the first step we have carried out DFT calculation for all structures under investigation. Next, the DFT total energies were fitted using third-order Birch-Murnaghan equation of state [51] for comparing with results of Ref. [28] where the same equation of state were used. The enthalpies calculated from the DFT total energy as the first step showed that the CsCl-type phase is unstable, which agrees with the previous study by Ono *et al.* [28], and the transition pressure from MnP-type ( $Pnma$ ) and  $Pm\bar{m}n$  phases is about 140 GPa.

Then we have taken into account on-site Coulomb repulsion within the DFT+DMFT method (Table I). Note that all phases under consideration at high pressures were obtained in the low spin (LS) and paramagnetic state. The magnitude of average squared local moment  $\langle m_z^2 \rangle$  is different from zero and decreases gradually with pressure, e.g., it is  $\sim 4 \mu_B^2$  at ambient pressure (AP) and  $1.8 \mu_B^2$  at  $\sim 400$  GPa for the CsCl-type phase. Similar behavior was observed for the  $Pnma$  phase ( $3.08$  and  $1.79 \mu_B^2$ ) and  $Pm\bar{m}n$  phase ( $2.56$  and  $1.87 \mu_B^2$ ) at AP and  $\sim 400$  GPa, respectively.

To check the accuracy of this calculation scheme we also calculated the critical pressure for the HS to LS transition in the  $Pnma$  phase. The result is shown in Fig. 3. The calculated transition pressure is about 10 GPa, which agrees well

TABLE I. Parameters of the Vinet equation of state obtained using DFT and DFT+DMFT calculations.

	Expt.	DFT	DFT+DMFT
<i>Pnma</i>			
$V_0, \text{\AA}^3$	99.5 [22]	96.24 [28]	99.79
$K_0, \text{GPa}$	156 [22]	175.7 [28]	147.16
$K'$	4 [22]	4.39 [28]	4.94
<i>Pm\bar{m}n</i>			
$V_0, \text{\AA}^3$	–	46.95 [28]	54.15
$K_0, \text{GPa}$	–	176 [28]	63.02
$K'$	–	4.35 [28]	6.34
CsCl type			
$V_0, \text{\AA}^3$	–	22.99 [11], 23.18 [19], 23.15 [28]	22.58
$K_0, \text{GPa}$	–	191 [11], 173.7 [19], 172.5 [28]	182.15
$K'$	–	4.11 [11], 4.55 [19], 4.54 [28]	5.08

with the experimental data (6.7 GPa at room temperature). Recently Ushakov *et al.* [23] have shown that a similar HS to LS transition in troilite (FeS I,  $P\bar{6}2c$  space group) can be reproduced by cell volume reduction.

As the next step we have taken into account vibrational contribution to the free energy, combining the results of the energy correction calculated within DFT+DMFT with results of phonon calculations in order to compute Gibbs free energies and construct the phase diagram in  $(P, T)$  coordinates.

The phase diagram calculated within the DFT+DMFT method, including vibrational effects, is shown in Fig. 4. Results of DFT with accounting for vibrational effect are reproduced from Ref. [30] and shown by gray dashed lines. The results of DFT+DMFT calculations which take into account vibrational effect are shown by black solid lines. The contribution of Coulomb correlation effect can be seen as the difference between results of these two methods. The DFT+DMFT results lie much closer to the experimental conditions of the phase transition from the  $Pnma$  phase to the CsCl type (186 GPa and 1300 K) [27]. It is known that the laser-heating method used in the experimental study has a significant temperature gradient in the sample [52,53] and therefore the experimental data had a big error ( $\gtrsim 300$  K).

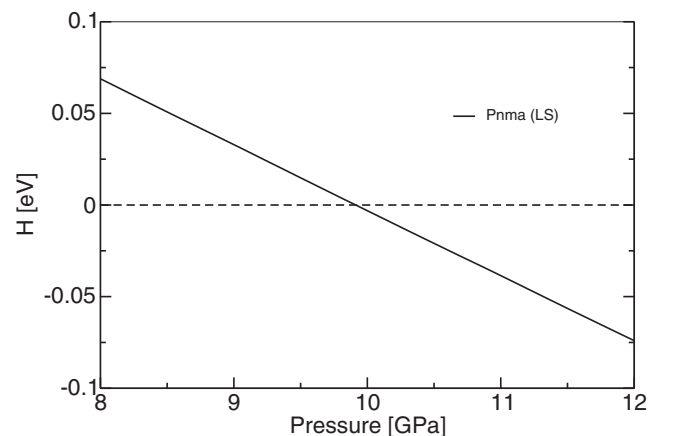


FIG. 3. Enthalpy difference between HS and LS states of the  $Pnma$  structure at  $T = 1160$  K calculated in DFT+DMFT.

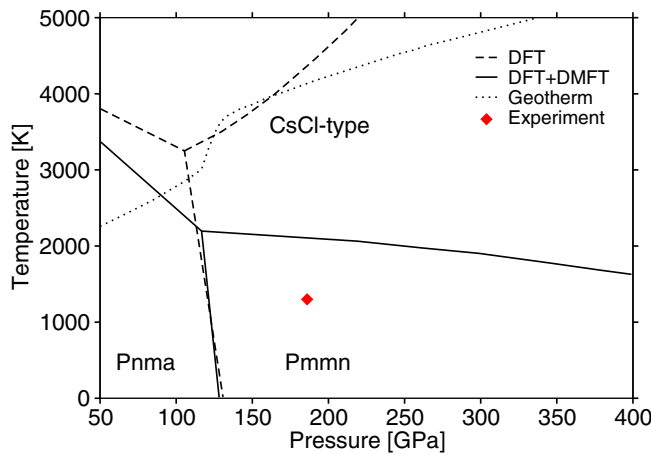


FIG. 4. Phase diagram as calculated within the DFT and DFT+DMFT methods, including vibrational effects. The temperature profile of the Earth (geotherm) is shown for reference. The experimental point of the CsCl-type phase [27] is marked with a red diamond.

However, the experimental points still lie in the computed stability field of the *Pmmn* phase. This discrepancy, albeit insignificant in this case, can be corrected by moderately adjusting the on-site Hubbard  $U$  (which was fixed in the present study, but should decrease slightly with pressure due to more effective screening) and Hund's intra-atomic exchange  $J_H$ . It was shown recently within DFT+DMFT method that calculated total energy and hence the critical pressure of phase transition were sensitive to the choice of Coulomb parameters [37,54]. Our results shows that the CsCl-type phase of FeS is stabilized by a combination of entropic and electron correlation effects, and that accounting for these effects one gets a dramatic improvement in the theoretical description of its stability in comparison with pure DFT calculations. The computed phase diagram shows that the correlation effects have a strong impact on the stability field of the

CsCl-type phase, leaving other transitions almost unchanged. We propose that such a selective effect could be related to the difference in coordination numbers. In the *Pmna* and *Pmmn* structures, iron has the same coordination number 6, whereas in the CsCl-type structure it is 8-coordinate. It seems plausible from our point of view, that phase transitions involving coordination number changes are particularly sensitive to electron correlation effects. Further investigation of possible interplay between change in coordination number of the strongly correlated atom and phase stability will require accurate charge self-consistent DFT+DMFT calculations.

#### IV. CONCLUSION

Unlike other known FeS phases which are well modeled in the DFT and DFT+ $U$  approximations, the CsCl-type structure could only be found to be stable after a thorough investigation with the thermal and electron correlation effects taken into consideration. However, modern computational techniques are capable of dealing with cases as subtle as this, displaying general agreement with experimental results.

By this means, we gain insight into the intriguing behavior of the iron sulfide exposed to high pressure. The calculated phase diagram gives a clue as to how to synthesize the *Pmmn* phase which has been predicted recently but still not seen in experiments: lower temperatures should be used. Our results show that electron correlations can play an important role even at very high pressures, such as pressures in the Earth's core, where local magnetic moments on iron atoms are suppressed but magnetic fluctuations are still significant.

#### ACKNOWLEDGMENTS

The DFT+DMFT calculations are supported by the Russian Science Foundation (grant 14-22-00004). Calculations of phonons and phase diagrams were performed with the support of the Russian Science Foundation (grant 16-13-10459).

- [1] J.-P. Poirier, *Phys. Earth Planet. Inter.* **85**, 319 (1994).
- [2] C. T. Seagle, A. J. Campbell, D. L. Heinz, G. Shen, and V. B. Prakapenka, *J. Geophys. Res.: Solid Earth* **111**, B06209 (2006).
- [3] Y. Fei, C. T. Prewitt, H. Mao, and C. M. Bertka, *Science* **268**, 1892 (1995).
- [4] T. Kamimura, M. Sato, H. Takahashi, N. Mori, H. Yoshida, and T. Kaneko, *J. Magn. Magn. Mater.* **104-107**, 255 (1992).
- [5] K. Kusaba, Y. Syono, T. Kikegawa, and O. Shimomura, *J. Phys. Chem. Solids* **58**, 241 (1997).
- [6] L. A. Taylor and H. K. Mao, *Science* **170**, 850 (1970).
- [7] H. Wang and I. Salveson, *Phase Trans.* **78**, 547 (2005).
- [8] H. E. King and C. T. Prewitt, *Acta Crystallogr. Sect. B* **38**, 1877 (1982).
- [9] D. M. Sherman, *Earth Planet. Sci. Lett.* **132**, 87 (1995).
- [10] H. Kobayashi, M. Sato, T. Kamimura, M. Sakai, H. Onodera, N. Kuroda, and Y. Yamaguchi, *J. Phys.: Condens. Matter* **9**, 515 (1997).
- [11] D. Alfè and M. J. Gillan, *Phys. Rev. B* **58**, 8248 (1998).
- [12] K. Kusaba, Y. Syono, T. Kikegawa, and O. Shimomura, *J. Phys. Chem. Solids* **59**, 945 (1998).
- [13] R. J. Nelmes, M. I. McMahon, S. A. Belmonte, and J. B. Parise, *Phys. Rev. B* **59**, 9048 (1999).
- [14] S. Takele and G. R. Hearne, *Phys. Rev. B* **60**, 4401 (1999).
- [15] J.-P. Rueff, C.-C. Kao, V. V. Struzhkin, J. Badro, J. Shu, R. J. Hemley, and H. K. Mao, *Phys. Rev. Lett.* **82**, 3284 (1999).
- [16] L. Vočadlo, D. Alfè, G. D. Price, and M. J. Gillan, *Phys. Earth Planet. Inter.* **120**, 145 (2000).
- [17] W. G. Marshall, R. J. Nelmes, J. S. Loveday, S. Klotz, J. M. Besson, G. Hamel, and J. B. Parise, *Phys. Rev. B* **61**, 11201 (2000).
- [18] A. Kavner, T. S. Duffy, and G. Shen, *Earth Planet. Sci. Lett.* **185**, 25 (2001).
- [19] P. Martin, G. Price, and L. Vočadlo, *Mineral. Mag.* **65**, 181 (2001).

- [20] S. Urakawa, K. Someya, H. Terasaki, T. Katsura, S. Yokoshi, K.-i. Funakoshi, W. Utsumi, Y. Katayama, Y. ichiro Sueda, and T. Irifune, *Phys. Earth Planet. Inter.* **143-144**, 469 (2004).
- [21] H. Kobayashi, T. Kamimura, D. Alfè, W. Sturhahn, J. Zhao, and E. E. Alp, *Phys. Rev. Lett.* **93**, 195503 (2004).
- [22] S. Ono and T. Kikegawa, *Am. Mineral.* **91**, 1941 (2006).
- [23] A. V. Ushakov, A. O. Shorikov, V. I. Anisimov, N. V. Baranov, and S. V. Streltsov, *Phys. Rev. B* **95**, 205116 (2017).
- [24] F. Keller-Besrest and G. Collin, *J. Solid State Chem.* **84**, 211 (1990).
- [25] H. King, D. Virgo, and H. K. Mao, *Carnegie Inst. Wash. Year Book* **77**, 830 (1978).
- [26] S. Ono, T. Kikegawa, and Y. Ohishi, *Eur. J. Mineral.* **19**, 183 (2007).
- [27] N. Sata, H. Ohfuji, K. Hirose, H. Kobayashi, Y. Ohishi, and N. Hirao, *Am. Mineral.* **93**, 492 (2008).
- [28] S. Ono, A. R. Oganov, J. P. Brodholt, L. Vočadlo, I. G. Wood, A. Lyakhov, C. W. Glass, A. S. Côté, and G. D. Price, *Earth Planet. Sci. Lett.* **272**, 481 (2008).
- [29] D. P. Dobson, L. Vočadlo, and I. G. Wood, *Am. Mineral.* **87**, 784 (2002).
- [30] Z. G. Bazhanova, V. V. Roizen, and A. R. Oganov, *Phys. Usp.* **60**, 1025 (2017).
- [31] K. Momma and F. Izumi, *J. Appl. Crystallogr.* **44**, 1272 (2011).
- [32] G. Kresse and J. Furthmüller, *Phys. Rev. B* **54**, 11169 (1996).
- [33] J. P. Perdew, K. Burke, and M. Ernzerhof, *Phys. Rev. Lett.* **77**, 3865 (1996).
- [34] V. I. Anisimov, A. I. Poteryaev, M. A. Korotin, A. O. Anokhin, and G. Kotliar, *J. Phys.: Condens. Matter* **9**, 7359 (1997).
- [35] K. Held, I. A. Nekrasov, G. Keller, V. Eyert, N. Blümer, A. K. McMahan, R. T. Scalettar, T. Pruschke, V. I. Anisimov, and D. Vollhardt, *Phys. Status Solidi B* **243**, 2599 (2006).
- [36] A. O. Shorikov, Z. V. Pchelkina, V. I. Anisimov, S. L. Skornyakov, and M. A. Korotin, *Phys. Rev. B* **82**, 195101 (2010).
- [37] J. Kuneš, A. V. Lukoyanov, V. I. Anisimov, R. T. Scalettar, and W. E. Pickett, *Nat. Mater.* **7**, 198 (2008).
- [38] A. O. Shorikov, A. V. Lukoyanov, V. I. Anisimov, and S. Y. Savrasov, *Phys. Rev. B* **92**, 035125 (2015).
- [39] N. A. Skorikov, A. O. Shorikov, S. L. Skornyakov, M. A. Korotin, and V. I. Anisimov, *J. Phys.: Condens. Matter* **27**, 275501 (2015).
- [40] P. Giannozzi, S. Baroni, N. Bonini, M. Calandra, R. Car, C. Cavazzoni, D. Ceresoli, G. L. Chiarotti, M. Cococcioni, I. Dabo, A. Dal Corso, S. de Gironcoli, S. Fabris, G. Fratesi, R. Gebauer, U. Gerstmann, C. Gougoussis, A. Kokalj, M. Lazzeri, L. Martin-Samos, N. Marzari, F. Mauri, R. Mazzarello, S. Paolini, A. Pasquarello, L. Paulatto, C. Sbraccia, S. Scandolo, G. Sclauzero, A. P. Seitsonen, A. Smogunov, P. Umari, and R. M. Wentzcovitch, *J. Phys.: Condens. Matter* **21**, 395502 (2009).
- [41] D. Korotin, A. V. Kozhevnikov, S. L. Skornyakov, I. Leonov, N. Binggeli, V. I. Anisimov, and G. Trimarchi, *Eur. Phys. J. B* **65**, 91 (2008).
- [42] A. I. Lichtenstein and M. I. Katsnelson, *Phys. Rev. B* **57**, 6884 (1998).
- [43] E. Gull, A. J. Millis, A. I. Lichtenstein, A. N. Rubtsov, M. Troyer, and P. Werner, *Rev. Mod. Phys.* **83**, 349 (2011).
- [44] A. Poteryaev, A. Belozero, A. Dyachenko, D. Korotin, M. Korotin, A. Shorikov, N. Skorikov, S. Skornyakov, and S. Streltsov, "AMULET," <http://amulet-code.org>.
- [45] V. I. Anisimov, D. M. Korotin, S. V. Streltsov, A. V. Kozhevnikov, J. Kuneš, A. O. Shorikov, and M. A. Korotin, *JETP Lett.* **88**, 729 (2009).
- [46] A. A. Dyachenko, A. O. Shorikov, A. V. Lukoyanov, and V. I. Anisimov, *Phys. Rev. B* **93**, 245121 (2016).
- [47] B. Amadon, S. Biermann, A. Georges, and F. Aryasetiawan, *Phys. Rev. Lett.* **96**, 066402 (2006).
- [48] A. Togo, F. Oba, and I. Tanaka, *Phys. Rev. B* **78**, 134106 (2008).
- [49] A. Togo and I. Tanaka, *Scr. Mater.* **108**, 1 (2015).
- [50] P. Vinet, J. R. Smith, J. Ferrante, and J. H. Rose, *Phys. Rev. B* **35**, 1945 (1987).
- [51] F. Birch, *Phys. Rev.* **71**, 809 (1947).
- [52] A. Dewaele, G. Fiquet, and P. Gillet, *Rev. Sci. Instrum.* **96**, 2421 (1998).
- [53] W. Panero and R. Jeanolz, *J. Appl. Phys.* **91**, 2769 (2002).
- [54] I. Leonov, *Phys. Rev. B* **92**, 085142 (2015).